Benchmarking of three-dimensional multicomponent lattice Boltzmann equation

XU, Xu <http://orcid.org/0000-0002-9721-9054>, BURGIN, Kallum, ELLIS, M and HALLIDAY, Ian <http://orcid.org/0000-0003-1840-6132>

Published version

XU, Xu, BURGIN, Kallum, ELLIS, M and HALLIDAY, Ian (2017). Benchmarking of three-dimensional multicomponent lattice Boltzmann equation. Physical Review E (PRE), 96 (5), 053308.

Benchmarking of three-dimensional multicomponent lattice Boltzmann equation

X. Xu,[1,2,*] K. Burgin,[1] M. A. Ellis,[3] and I. Halliday[1]
[1]*Materials & Engineering Research Institute, Sheffield Hallam University, Howard Street, S1 1WB, UK*
[2]*Department of Engineering and Mathematics, Sheffield Hallam University, Howard Street, S1 1WB, UK*
[3]*Oriel College, University of Oxford, OX1 4EW, UK*

(Received 17 August 2017; revised manuscript received 25 October 2017; published 15 November 2017)

We present a challenging validation of phase field multicomponent lattice Boltzmann equation (MCLBE) simulation against the Re = 0 Stokes flow regime Taylor-Einstein theory of dilute suspension viscosity. By applying a number of recent advances in the understanding and the elimination of the interfacial microcurrent artefact, extending to a three-dimensional class of stability-enhancing multiple relaxation time collision models (which require no explicit collision matrix, note) and developing new interfacial interpolation schemes, we are able to obtain data that show that MCLBE may be applied in new flow regimes. Our data represent one of the most stringent tests yet attempted on LBE—one which received wisdom would preclude on grounds of overwhelming artefact flow.

DOI: 10.1103/PhysRevE.96.053308

I. INTRODUCTION

The past two decades have seen steady growth in interest in multirelaxation time (MRT) lattice Boltzmann (LB) schemes, which offer enhanced simulation stability [1–8], etc. We extend to D3Q19 a recent D2Q9 variant [9], in which the usual collision matrix is only implicit, being represented by a carefully chosen, modal eigenbasis, which is subject to forced, scalar relaxation. As well as the usual advantages, the new method has transparent analytic properties: its orthogonal modes are defined as polynomials in the lattice basis, as are the elements of the transformation matrix between the distribution function and the mode space. This uniquely allows for the direct reconstruction of a post-collision distribution function, which is effectively parameterized by the eigenvalue spectrum. Our purpose in developing a new model is to stabilize multicomponent LBE (MCLBE) so as to attempt the challenge of recovering the Taylor-Einstein theory of suspension viscosity [10,11].

The structure of this paper is as follows. In Sec. II, we provide background material of the proposed 3D MRT scheme. In Sec. III, we present relevant methodological advances, in particular, the discovery of 19 polynomial expressions for the inverse transformation matrix, and the analysis of different viscosity interpolation methods. In Sec. IV, we illustrate and discuss the theoretical and simulation results achieved and finally, in Sec. V, we conclude on the significant findings of this work.

II. BACKGROUND

First, consider the base model. Our three-dimensional (3D) MRT LBE with body force, **F**, may be written

$$f_i(\mathbf{x}+\mathbf{c_i}\delta t, t+\delta t) = f_i(\mathbf{x},t) + \sum_j A_{ij}\left[f_j^{(0)}(\mathbf{x},t) - f_j(\mathbf{x},t)\right] + \delta t F_i, \quad (1)$$

where

$$F_i = t_i\left[3\mathbf{F}\cdot\mathbf{c}_i + \frac{9}{2}\left(1-\frac{\lambda_3}{2}\right)(F_\alpha u_\beta + F_\beta u_\alpha)\right], \quad (2)$$

and

$$f_j^{(0)} = \rho t_j\left(1 + 3u_\alpha c_{j\alpha} + \tfrac{9}{2}u_\alpha u_\beta c_{j\alpha}c_{j\beta} - \tfrac{3}{2}u_\gamma u_\gamma\right). \quad (3)$$

To recover hydrodynamics, F_i, collision matrix **A**, and its eigenvalues λ_i, must preserve the following properties:

$$\sum_i F_i = 0, \quad \sum_i \mathbf{c}_i F_i = n\mathbf{F}, \quad \sum_i \mathbf{c}_i\mathbf{c}_i F_i = \frac{1}{2}[\mathbf{C}+\mathbf{C}^{\mathbf{T}}],$$
$$\sum_i 1_i A_{ij} = 0, \quad \sum_i c_{i\alpha}A_{ij} = 0, \quad \sum_i g_i A_{ij} = \lambda_{10} g_j,$$
$$\sum_i c_{i\alpha}c_{i\beta}A_{ij} = \lambda_4 c_{j\alpha}c_{j\beta}, \quad \sum_i g_i c_{i\alpha}A_{ij} = \lambda_{11} g_j c_{j\alpha},$$
$$\sum_i c_{i\alpha}^2 c_{i\beta}A_{ij} = \lambda_{14} c_{j\alpha}^2 c_{j\beta}, \quad \sum_i g_i c_{i\alpha}^2 A_{ij} = \lambda_{17} g_j c_{j\alpha}^2, \quad (4)$$

where α and β represent the x, y, or z directions, λ_p denotes the pth eigenvalue of A_{ij}, and $C_{\alpha\beta} \equiv \frac{1}{2}(u_\alpha F_\beta + u_\beta F_\alpha)$ [9]. For eigenvalues, their corresponding left-row eigenvectors, $\mathbf{h}^{(p)}$, $p \in [0,18]$, and the modes they project, see Table I(a). **A** is defined by its eigenspectrum $(\mathbf{h}^{(p)},\lambda_p)$, which project modes with scalar relaxation.

III. METHODOLOGY

A. Explicit algebraic 3D MRT scheme

For D3Q19, we extend the set developed for D2Q9 [9], using Gram-Schmidt orthogonalization to which in Table I(a). Four degenerate eigenvectors necessarily project hydrodynamic modes $\rho \equiv \sum_i f_i$ and $\rho\mathbf{u} \equiv \sum_i f_i\mathbf{c}_i$ [9] with $\lambda_i = 0$, six project components of stress $P_{\alpha\beta}$, four "ghosts" are chosen to project N, **J** (following Refs. [2–4]) and five new eigenvectors are denoted E_1, E_2, E_3, X_x, and X_y. Left-row eigenvectors $\mathbf{h}^{(p)}s$ define projection matrix

$$\mathbf{M} \equiv (\mathbf{h}^{(0)},\mathbf{h}^{(1)},\ldots,\mathbf{h}^{(18)})^T, \quad (5)$$

*Author to whom all correspondence should be addressed: xu.xu@shu.ac.uk

TABLE I. (a) Collision matrix left-row eigenvector notation and properties, with eigenvalues and the corresponding equilibria and sources used in Eq. (9). Here, ρu_α, $P_{\alpha\beta}$, and $\Pi^{(0)}_{\alpha\beta}$ represent the α and $\alpha\beta$ components of momentum, viscous stress tensor, and momentum flux tensor, respectively. (b) The lattice basis or unit cell set for the D3Q19 model developed in this paper.

(a)						(b)			
Mode	Component	λ_p	Projection	Modal source, $S^{(p)}$	Equilibrium, $s^{(p)}$	Direction, i	c_{ix}	c_{iy}	c_{iz}
$\mathbf{h}^{(0)}$	$h_i^{(0)} = 1_i$	0	ρ	0	ρ	0	0	0	0
$\mathbf{h}^{(1)}$	$h_i^{(1)} = c_{ix}$	0	ρu_x	$nF_x\delta_t$	ρu_x	1	1	0	0
$\mathbf{h}^{(2)}$	$h_i^{(2)} = c_{iy}$	0	ρu_y	$nF_y\delta_t$	ρu_y	2	1	−1	0
$\mathbf{h}^{(3)}$	$h_i^{(3)} = c_{iz}$	0	ρu_z	$nF_z\delta_t$	ρu_z	3	0	−1	0
$\mathbf{h}^{(4)}$	$h_i^{(4)} = c_{ix}^2$	λ_4	P_{xx}	$\frac{1}{2}(C_{xx} + C_{xx})$	$\Pi^{(0)}_{xx}$	4	−1	−1	0
$\mathbf{h}^{(5)}$	$h_i^{(5)} = c_{iy}^2$	λ_4	P_{yy}	$\frac{1}{2}(C_{yy} + C_{yy})$	$\Pi^{(0)}_{yy}$	5	−1	0	0
$\mathbf{h}^{(6)}$	$h_i^{(6)} = c_{iz}^2$	λ_4	P_{zz}	$\frac{1}{2}(C_{zz} + C_{zz})$	$\Pi^{(0)}_{zz}$	6	−1	1	0
$\mathbf{h}^{(7)}$	$h_i^{(7)} = c_{ix}c_{iy}$	λ_4	P_{xy}	$\frac{1}{2}(C_{xy} + C_{yx})$	$\Pi^{(0)}_{xy}$	7	0	1	0
$\mathbf{h}^{(8)}$	$h_i^{(8)} = c_{ix}c_{iz}$	λ_4	P_{xz}	$\frac{1}{2}(C_{xz} + C_{zx})$	$\Pi^{(0)}_{xz}$	8	1	1	0
$\mathbf{h}^{(9)}$	$h_i^{(9)} = c_{iy}c_{iz}$	λ_4	P_{yz}	$\frac{1}{2}(C_{yz} + C_{zy})$	$\Pi^{(0)}_{yz}$	9	0	0	1
$\mathbf{h}^{(10)}$	$h_i^{(10)} = g_i$	λ_{10}	N	0	0	10	1	0	1
$\mathbf{h}^{(11)}$	$h_i^{(11)} = g_ic_{ix}$	λ_{11}	J_x	0	0	11	0	1	1
$\mathbf{h}^{(12)}$	$h_i^{(12)} = g_ic_{iy}$	λ_{11}	J_y	0	0	12	−1	0	1
$\mathbf{h}^{(13)}$	$h_i^{(13)} = g_ic_{iz}$	λ_{11}	J_z	0	0	13	−1	0	1
$\mathbf{h}^{(14)}$	$h_i^{(14)} = c_{ix}^2c_{iy}$	λ_{14}	E_1	$\frac{1}{3}F_y$	$E_1^{(0)} = \frac{1}{3}\rho u_y$	14	0	0	−1
$\mathbf{h}^{(15)}$	$h_i^{(15)} = c_{ix}^2c_{iz}$	λ_{14}	E_2	$\frac{1}{3}F_z$	$E_2^{(0)} = \frac{1}{3}\rho u_z$	15	1	0	−1
$\mathbf{h}^{(16)}$	$h_i^{(16)} = c_{ix}c_{iy}^2$	λ_{14}	E_3	$\frac{1}{3}F_x$	$E_3^{(0)} = \frac{1}{3}\rho u_x$	16	0	1	−1
$\mathbf{h}^{(17)}$	$h_i^{(17)} = g_ic_{ix}^2$	λ_{17}	X_x	$\left(1 - \frac{\lambda_4}{2}\right)(F_yu_y + F_zu_z)$	$X_x^{(0)} = \frac{\rho}{2}\left(u_y^2 + u_z^2\right)$	17	−1	0	−1
$\mathbf{h}^{(18)}$	$h_i^{(18)} = g_ic_{iy}^2$	λ_{17}	X_y	$\left(1 - \frac{\lambda_4}{2}\right)(F_xu_x + F_zu_z)$	$X_y^{(0)} = \frac{\rho}{2}\left(u_x^2 + u_z^2\right)$	18	0	−1	−1

such that

$$\mathbf{M}\,\mathbf{f} = (\rho, \rho u_x, \rho u_y, \rho u_z, P_{xx}, P_{yy}, P_{zz}, P_{xy}, P_{xz}, P_{yz}, N, J_x, J_y, J_z, E_1, E_2, E_3, X_x, X_y)^T, \quad (6)$$

where $\mathbf{f} \equiv (f_0, f_1, f_2, \ldots, f_{18})^T$. Using $\mathbf{M}$, Eq. (1) may be transformed to

$$\mathbf{M}\,\mathbf{f}^+ = \mathbf{M}\,\mathbf{f} + \mathbf{M}\,\mathbf{A}\,\mathbf{M}^{-1}(\mathbf{M}\,\mathbf{f}^{(0)} - \mathbf{M}\,\mathbf{f}) + \mathbf{M}\tilde{\mathbf{F}}, \quad (7)$$

where $\tilde{\mathbf{F}}$ denotes a column vector with elements F_i and $\mathbf{f}$, $\mathbf{f}^+$ and $\mathbf{f}^{(0)}$ are now column vectors. Since the $\mathbf{h}^{(p)}$ are left row eigenvectors of $\mathbf{A}$, it follows

$$\mathbf{M}\,\mathbf{A} = \Lambda\,\mathbf{M} \;\Leftrightarrow\; \Lambda = \mathbf{M}\,\mathbf{A}\,\mathbf{M}^{-1}, \quad (8)$$

where $\Lambda = \mathrm{diag}(\lambda_0, \lambda_1, \ldots, \lambda_{18})$. Therefore, Eq. (1) may be written in mode space as

$$\mathbf{h}^{(p)+} = \mathbf{h}^{(p)} + \lambda_p(\mathbf{s}^{(p)} - \mathbf{h}^{(p)}) + \mathbf{S}^{(p)}, \quad (9)$$

where $\mathbf{S}^{(p)} \equiv \mathbf{M} \cdot \tilde{\mathbf{F}}$ and $\mathbf{s}^{(p)} \equiv \mathbf{M} \cdot \mathbf{f}^{(0)}$. The inverse transformation matrix,

$$\mathbf{M}^{-1} \equiv (\mathbf{k}^{(0)}, \mathbf{k}^{(1)}, \mathbf{k}^{(2)}, \ldots, \mathbf{k}^{(18)}), \quad (10)$$

may be constructed from column vectors $\mathbf{k}^{(p)}$, exactly defined as polynomials of the lattice basis, such that

$$6k_i^{(0)} = t_i\left[12g_ic_{i\theta}^2 - 15c_{i\theta}^2 - 21c_{iz}^2 + 23 - 8g_i\right], \quad (11)$$

$$k_i^{(1)} = t_i[6c_{ix}c_{iy}(2c_{ix} - c_{iy}) + c_{ix}(5 + g_i) - 2c_{iy}(2 - g_i)], \quad (12)$$

$$k_i^{(2,3)} = t_ic_{i\gamma}\left[5 + g_i - 6c_{ix}^2\right], \quad (13)$$

$$2k_i^{(4,5)} = t_i\left[-2g_i\left(c_{i\zeta}^2 + 2c_{i\xi}^2\right) + 11c_{i\zeta}^2 + c_{i\xi}^2 + 3c_{iz}^2 - 5 + 2g_i\right], \quad (14)$$

$$2k_i^{(6)} = t_i\left[-6g_ic_{i\theta}^2 + 3c_{i\theta}^2 + 15c_{iz}^2 - 7 + 4g_i\right],$$
$$k_i^{(7,\ldots,9)} = 3t_ic_{i\alpha}c_{i\beta}, \quad (15)$$

$$2k_i^{(10)} = t_i\left[6c_{i\theta}^2 - 12g_ic_{i\theta}^2 + 12c_{iz}^2 - 8 + 11g_i\right], \quad (16)$$

$$k_i^{(11)} = t_i[3c_{ix}c_{iy}(2c_{ix} - c_{iy}) + c_{ix}(1 + 2g_i) - c_{iy}(2 + g_i)], \quad (17)$$

$$k_i^{(12,13)} = 2t_ig_ic_{i\gamma}\left[2 + 4g_i - 6c_{ix}^2\right], \quad (18)$$

$$k_i^{(14,15)} = 3t_ic_{i\gamma}\left[6c_{ix}^2 - 2 - g_i\right], \quad (19)$$

$$k_i^{(16)} = 3t_i[6c_{ix}c_{iy}(c_{iy} - 2c_{ix}) - (2 + g_i)(c_{ix} - 2c_{iy})], \quad (20)$$

$$k_i^{(17)} = t_i\left[-g_i\left(4c_{ix}^2 + c_{iy}^2\right) - c_{ix}^2 - 2c_{iy}^2 - 3c_{iz}^2 + 2 - 2g_i\right], \quad (21)$$

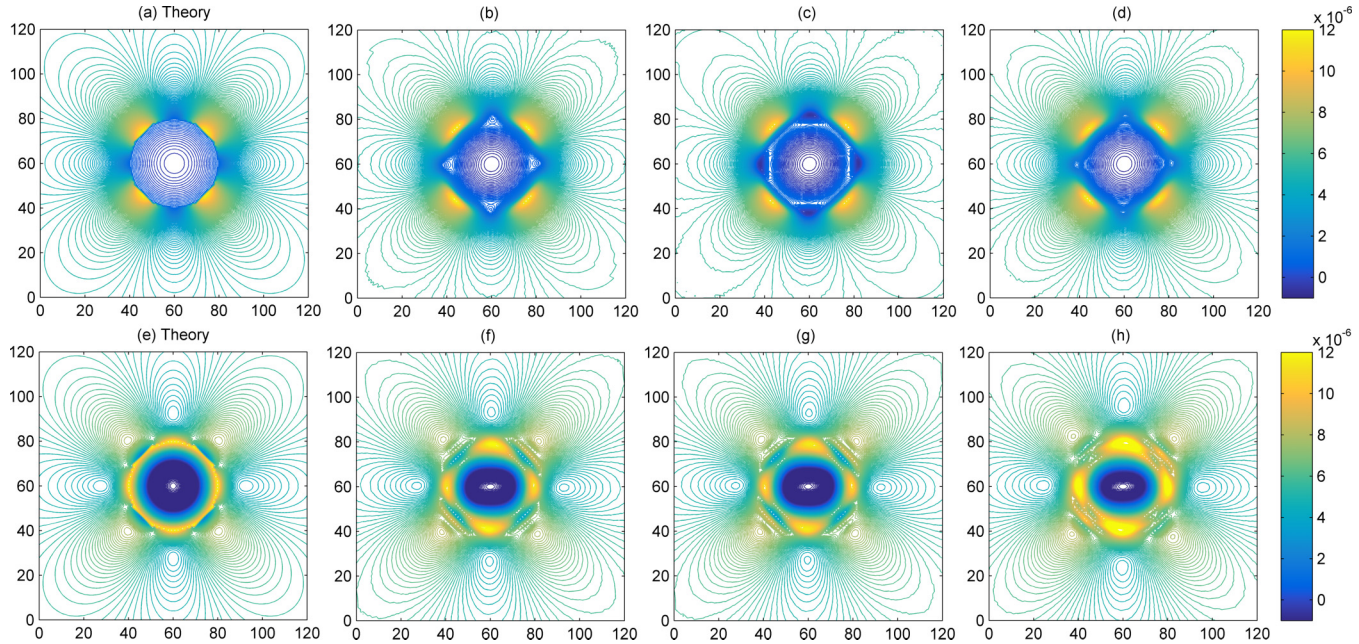

FIG. 1. Viscous stress field σ'_{xy} in the equatorial plane of a spherical red drop, radius $R = 20$, suspended in a blue fluid which is sheared, at Re $= 0$ for two viscosity ratios, Λ, with $\eta_B = \frac{1}{3}$ (continuous component) and $\frac{R}{L} = \frac{1}{6}$. Case 1, $\Lambda = \frac{1}{16}$: (a) Taylor's theory, (b) interfacial interpolation based upon a density-weighted harmonic mean of separated fluids' parameter $\tau = \frac{1}{\lambda_4}$ [see Eq. (27)], (c) interfacial interpolation based upon a density-weighted harmonic mean of shear viscosity [see Eq. (28)], and (d) interfacial interpolation based upon a density-weighted arithmetic mean of shear viscosity [see Eq. (29)]. Case 2, $\Lambda = 12$: (e) Taylor's theory, (f) interfacial interpolation based upon a density-weighted harmonic mean of separated fluids' parameter $\tau = \frac{1}{\lambda_4}$ [see Eq. (27)], (g) interfacial interpolation based upon a density-weighted harmonic mean of shear viscosity [see Eq. (28)], and (h) interfacial interpolation based upon a density-weighted arithmetic mean of shear viscosity [see Eq. (29)].

$$k_i^{(18)} = t_i\left[2g_i\left(c_{ix}^2 + 2c_{iy}^2\right) - 2c_{ix}^2 - c_{iy}^2 - 3c_{iz}^2 + 2 - 2g_i\right], \tag{22}$$

where $c_{i\theta}^2 = c_{ix}^2 + c_{iy}^2$, $\gamma \in [y,z]$ and is taken in alphabetical order, (ζ,ξ) are taken in order as (x,y) and (y,x), and $\alpha,\beta \in [x,y,z]$ are denoted in the pair order of (x,y), (x,z), and (y,z). Using the methodology developed for the D2Q9 case [9], we invert $\mathbf{M}$ to construct a post-collision distribution function vector $\mathbf{f}^+$, describing flow in the presence of force distribution, $\mathbf{F}$:

$$\mathbf{f}^+ = \mathbf{M}^{-1}(\rho^+, \rho u_x^+, \rho u_y^+, \rho u_z^+, P_{xx}^+, P_{yy}^+, P_{zz}^+, P_{xy}^+, P_{xz}^+, P_{yz}^+, N^+, J_x^+, J_y^+, J_z^+, E_1^+, E_2^+, E_3^+, X_x^+, X_y^+)^T, \tag{23}$$

which may be written in explicit form after Ref. [9]. MRT LBE is more computationally expensive than LBGK [12] but is more stable [1–3]. The scheme we extend here from Ref. [9] includes the existence of polynomial expressions $\mathbf{k}^{(p)}$, which allow (i) algebraic inversion from the mode space [Eq. (10)], (ii) an exact expression for $\mathbf{f}^+$, (iii) removal of explicit collision and inversion matrices, and hence some computational overhead.

B. Interfacial viscosity interpolation

Here we are motivated by a need to extend the viscosity contrast available in simulations of multicomponent flow using a phase-field MCLBE [9,13,14], to facilitate a validation against the stress field Taylor predicted in 1932, for steady, shear flow past a spherical drop at Re $= 0$ [10] and the consequent prediction of effective viscosity in a dilute suspension of small drops, after Einstein [11]. Accordingly,

$$\mathbf{F} = \frac{\sigma\kappa}{2}\nabla\rho^N \tag{24}$$

is an immersed boundary force, where according to Ref. [15], the phase field is

$$\rho^N \equiv \frac{\rho_R - \rho_B}{\rho_R + \rho_B}, \tag{25}$$

and the local interfacial curvature is

$$\kappa \equiv \nabla_s \frac{\nabla\rho^N}{|\nabla\rho^N|}. \tag{26}$$

Here, ρ_R and ρ_B are densities of two immiscible fluid components, which are segregated, post collision, using the methodology of d'Ortona [16] (see Refs. [9,13,14]) and ∇_s is a surface gradient operator.

The above force field is localized but clearly continuously distributed. In fact, in all MCLBE an interface is defined by a phase field or order parameter, which varies continuously, over a small distance, between constant bulk fluids values, with a continuum interface commonly taken to be $\rho_N = 0$ surface. The finite width of the resulting interface calls into question the representation of target continuum-scale kinematic and

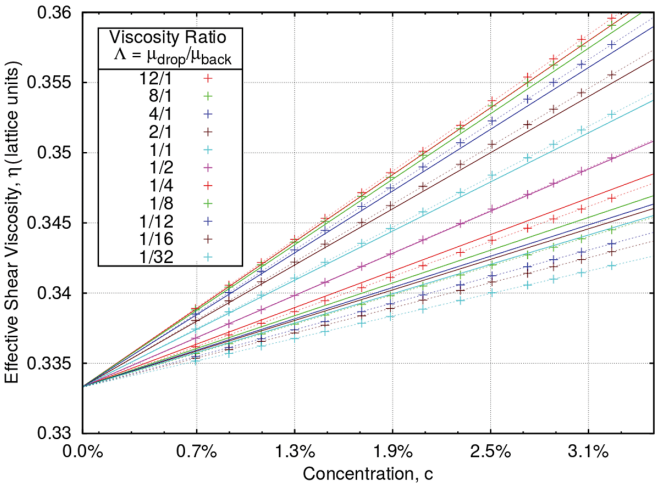

FIG. 2. Effective suspension viscosity, η_{eff}, as a function of concentration, c (discrete crosses linearly interpolated by dotted lines), for the indicated range of drop/background fluid viscosity ratio, $\Lambda = \frac{\eta_R}{\eta_B}$, together with the variation predicted by the Taylor-Einstein result, $\eta_{\text{eff}}^{(T)} = \eta_B[1 + (\frac{\frac{5}{2}\eta_R+\eta_B}{\eta_R+\eta_B})c]$ (continuous line of corresponding color). These data were obtained using the interpolation defined in Eq. (27).

dynamic conditions. In the present context, we are concerned with the no-traction condition [17].

Take a steady, planar, red-blue interface $x = x_0$, constant, sheared in y direction, after Liu *et al.* [18]. Phase field MCLBE is described by a weakly compressible Navier-Stokes equation with $\mathbf{F}$, for what is a single, effective fluid (the role of $\mathbf{F}$ is to insert Laplace law physics). For a flat interface, $\mathbf{F} = \mathbf{0}$ and the lattice fluid is described by $\frac{d}{dx}\sigma'_{xy} = 0, \forall x$. Applying system symmetries, we obtain $\sigma'_{xy} = K$, a constant $\forall x$. This prefigures the continuum no-traction (continuity of viscous flux) condition. Apparently, LBE's dynamics automatically ensure shear stress is continuous through the interface region. Clearly, choice exists in the interpolation of viscosity or, equivalently, λ_4. Liu and coworkers impose a requirement on the velocity gradient, which it varies like ρ^N [18], in this situation and in applications to contact angle hysteresis [19]. This assumption yields an interpolation of λ_4 derived from the harmonic mean of viscosity with weights $\frac{\rho_R}{\rho}$ and $\frac{\rho_B}{\rho}$. Liu *et al.* [18] state their approach is equivalent to Ginzburg's, when projecting the sharp interface limit [20] (see Fig. 3 of Ref. [20]). Zu *et al.* [21] assume the interfacial velocity gradient follows an order parameter and argue for an interpolation based on a weighted arithmetic average of reciprocal viscosity. There are more involved approaches, including that of Grunau *et al.* [22]. For the data presented in the next section, optimum agreement with Taylor-Einstein theory is obtained using an alternative method.

In our MCLBE, interfacial effects are carried by a force with weight $|\nabla\rho^N|$, which may be approximated by $\frac{4\rho_R\rho_B}{\rho^2} = (1-\rho^{N2})$ [23]. Self-consistency argues for an interpolation of λ_4, between bulk values λ_4^R and λ_4^B, such that source term, F_i, has a consistent variation. Hence, we choose $(1-\frac{\lambda_4}{2}) \sim \rho^N$ or $(1-\frac{\bar{\lambda}_4}{2}) = \frac{\rho_R}{\rho}(1-\frac{\lambda_4^R}{2}) + \frac{\rho_B}{\rho}(1-\frac{\lambda_4^B}{2})$, and noting $\frac{\rho_R}{\rho} + \frac{\rho_B}{\rho} = 1$, our interpolation may be written

$$\bar{\lambda}_4 = \frac{\rho_R}{\rho}\lambda_4^R + \frac{\rho_B}{\rho}\lambda_4^B = \frac{1+\rho^N}{2}\lambda_4^R + \frac{1-\rho^N}{2}\lambda_4^B. \quad (27)$$

In Sec. IV we will consider data derived from the above interpolation alongside that obtained using other methods. The different interpolations used for reference in Sec. IV are based on taking a relative density weighted harmonic mean of shear viscosity $\eta = \frac{\rho}{\frac{\rho_R}{\eta_R}+\frac{\rho_B}{\eta_B}}$, which may be expressed as follows:

$$\frac{\bar{\lambda}_4}{2-\bar{\lambda}_4} = \frac{\rho_R}{\rho}\left(\frac{\lambda_4^R}{2-\lambda_4^R}\right) + \frac{\rho_B}{\rho}\left(\frac{\lambda_4^B}{2-\lambda_4^B}\right), \quad (28)$$

and also an interpolation based on the arithmetic mean of shear viscosity $\eta = \frac{\rho_R}{\rho}\eta_R + \frac{\rho_B}{\rho}\eta_B$, which may be expressed as

$$\frac{1}{\bar{\lambda}_4} = \frac{\rho_R}{\rho}\frac{1}{\lambda_4^R} + \frac{\rho_B}{\rho}\frac{1}{\lambda_4^B}. \quad (29)$$

IV. RESULTS AND DISCUSSION

Experimental studies of suspension viscosity emphasize concentration values outside the Re = 0 theory but do identify certain emulsions that behave in agreement with the Taylor-Einstein result, certainly for concentrations $c < 5\%$ (see, e.g., Nawab *et al.* [24], Hur *et al.* [25], and Mason *et al.* [26]). Notably, a comparison of MCLBE with Re = 0 theory is not obstructed by MCLBE's notorious interfacial microcurrent (see Ref. [27] and references therein). For phase-field MCLBE variants, this artefact has recently been argued to arise from superposable solutions to the field equations, attributable, in increasing significance, to the stencil used for force weight $\nabla\rho^N$, discrete lattice effects, and (most significantly) the calculation of κ [27]. At Re = 0, hydrodynamic signals cannot be assumed to overwhelm artefacts, but this regime may still be addressed by subtracting independent microcurrent fields, to expose a hydrodynamic response. (Micro-current fields are easily determined for a red drop in stationary blue fluid.)

Figure 1 compares stresses between theory and microcurrent adjusted simulation. We show viscous stress σ'_{xy} measured in the projected equatorial plane, $z = 0$, of a three-dimensional red drop, initial radius $R = 20$ lattice units, contained within a cubic box, side L lattice units, with the continuous component (blue) fluid subject to a Lees-Edwards shear [28]. This boundary condition eliminates finite-size effects but allows periodic drop replicas to interact [9]. The resulting suspension concentration is controlled by L, i.e.,

$$c = \frac{4\pi R^3}{3L^3}. \quad (30)$$

The applied shear corresponds to approximately constant boundary flow parallel to $\hat{e}_y$ in box faces $x = x_0$, constant. Taylor calculated $\sigma'^{(T)}_{\alpha\beta}$, $\alpha,\beta \in [x,y,z]$ due to an inclined, applied shear, superposed with a constant body rotation around $\hat{e}_z$ [10]. Accordingly, to compare with our simulation, it is necessary to rotate coordinates and Fig. 1(a) shows a combination of Taylor's stresses $(\sigma'^{(T)}_{xx} - \sigma'^{(T)}_{yy})$. Figures 1(b)–1(d) show the corresponding simulation data for

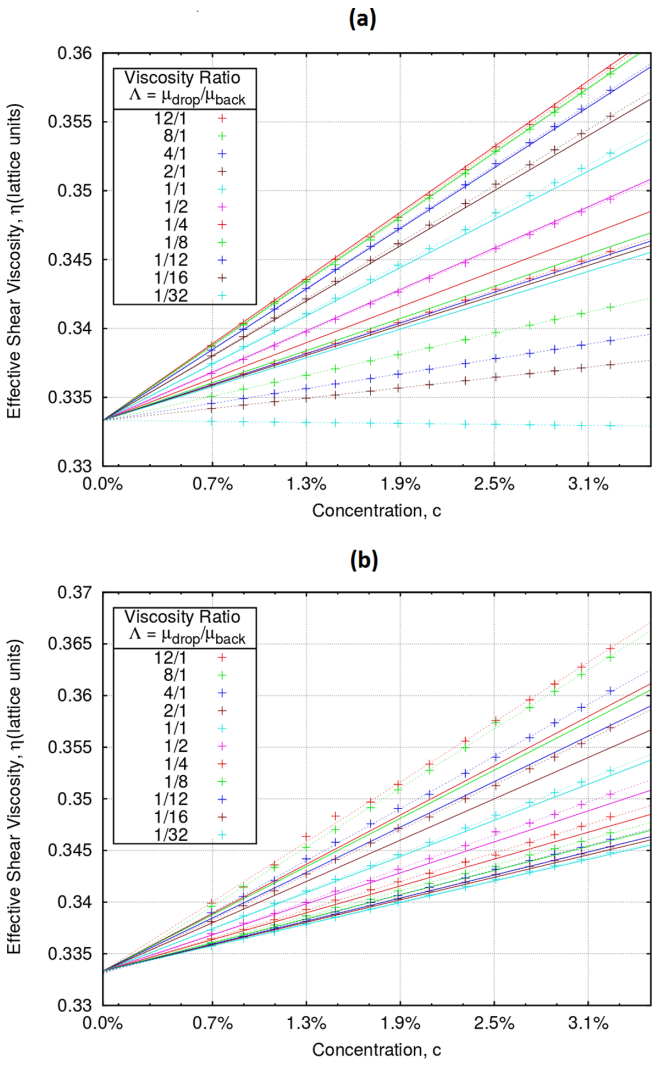

FIG. 3. Data equivalent to that shown in Fig. 2 using different interfacial interpolation methods. Effective suspension viscosity, η_{eff}, as a function of concentration, c (discrete crosses linearly interpolated by dotted lines), for the indicated range of drop/background fluid viscosity ratio, $\Lambda = \frac{\eta_R}{\eta_B}$, together with the variation predicted by the Taylor-Einstein result, $\eta_{\text{eff}}^{(T)} = \eta_B[1 + (\frac{\frac{5}{2}\eta_R+\eta_B}{\eta_R+\eta_B})c]$ (continuous line of corresponding color). These data were obtained using an interpolation based upon (a) the harmonic mean of the separated fluids' shear viscosity defined in Eq. (28) and (b) the arithmetic mean of shear viscosity defined in Eq. (29).

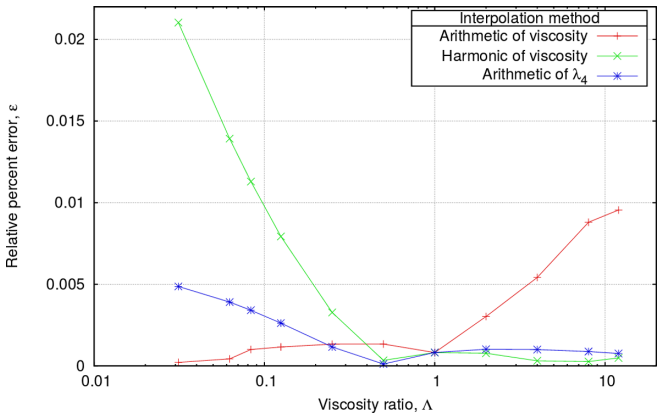

FIG. 4. Relative error of interfacial interpolation method, ϵ, for a range of Λ, expressed in percentage. For all data in Fig. 2, $\epsilon \equiv \frac{\eta_{\text{eff}}^{(T)} - \eta_{\text{eff}}}{\eta_{\text{eff}}^{(T)}} \times 100\%$ was computed for each of the three interfacial interpolation methods considered, as identified in the key.

$L = 128$, viscosity contrast:

$$\Lambda \equiv \frac{\eta_R}{\eta_B}, \tag{31}$$

where η_C is the shear viscosity of the C fluid. In Fig. 1 we show the significant difference between stress fields measured using existing and alternative interfacial interpolations of viscosity, or equivalently, λ_4. These are given in Eqs. (27), (28), and (29). Furthermore, the viscous stress field, σ'_{xy}, is shown in Fig. 1 for two Λ. For this data, $\eta_B = \frac{1}{3}$ (the continuous component) is fixed and $\frac{R}{L} = \frac{1}{6}$. For the images in the upper row, $\Lambda = \frac{1}{16}$. Figure 1(a) shows Taylor-Einstein theory; Fig. 1(b) shows the stress field obtained using the interfacial interpolation based upon a density-weighted harmonic mean of separated fluids' parameter $\tau = \frac{1}{\lambda_4}$ [see Eq. (27)]; Fig. 1(c) shows stress obtained with the interfacial interpolation based upon a density-weighted harmonic mean of shear viscosity [see Eq. (28); and Fig. 1(d) shows results from our method of interfacial interpolation shear viscosity, based upon a density-weighted arithmetic mean of shear viscosity [see Eq. (29)]. In the top row, it is clear that Figs. 1(b) and 1(d) are most representative of Fig. 1(a). The bottom row in Fig. 1 shows equivalent data for $\Lambda = 12$ and it clearly shows that Figs. 1(f) and 1(g) are most representative of Fig. 1(e).

We next consider a range of crystalline suspension concentrations, each of fixed viscosity ratio, Λ, inferring effective suspension viscosity, η_{eff}, from plots of system-averaged $\langle\sigma_{xy}\rangle$ against c, fitted using unconstrained regression (see, e.g., Fig. 2). For microcurrent flow alone, $\langle\sigma_{xy}\rangle \approx 0$ (though viscous dissipation is affected—see Ref. [9]) but it is still necessary to correct system $\langle\sigma_{xy}\rangle$ for the presence of immersed boundary force, $\mathbf{F}$ [9]. Agreement with Taylor-Einstein theory is affected by the method used to interpolate λ_4, or alternatively viscosity, η, in the interfacial region, as we now discuss. All data in Figs. 2, 3, and 4 correspond to

$$\text{Re} \equiv \frac{\dot{\gamma} R^2 \rho}{\eta} = 0.0198, \tag{32}$$

$$\text{Ca} \equiv \frac{\eta \dot{\gamma} R}{\sigma} = 0.0110, \tag{33}$$

which are held constant throughout.

Figure 2 shows 11 sets of measured η_{eff} for a wide range of Λ such that $\frac{1}{32} \leqslant \Lambda \leqslant 12$ (crosses interpolated by dotted lines), and the appropriate Taylor-Einstein predictions (solid lines of same color):

$$\eta_{\text{eff}}^{(T)} = \eta_B \left[1 + \left(\frac{\frac{5}{2}\Lambda + 1}{\Lambda + 1}\right)c\right]. \tag{34}$$

Data presented in Fig. 3 are equivalent to that shown in Fig. 2, but using different interfacial interpolation methods.

Figure 3(a) shows effective suspension viscosity data based upon the interpolation of interfacial viscosity in Eq. (28); Fig. 3(b) shows equivalent data based upon Eq. (29). The quality of the fit to theory with the different interpolation methods is different over different part over the domain of Λ. This is clearly shown in Fig. 4, where we show the relative error,

$$\epsilon \equiv \left(\frac{\eta_{\text{eff}}^{(T)} - \eta_{\text{eff}}}{\eta_{\text{eff}}^{(T)}} \right) \times 100\%, \tag{35}$$

plotted over the range of Λ. It is apparent that for $\Lambda > 1$, the agreement with theory using arithmetic mean method is significantly worse, whereas for $\Lambda < 1$, the agreement using harmonic mean method is much worse. Our interpolation in Eq. (27) represents an optimum over the whole range of Λ. This point is further summarized in Sec. V.

V. CONCLUSIONS

Taken together, Figs. 1–4 underscore the significance of the interfacial interpolation. The fit produced by Eq. (27) represents an optimum over the range of Λ studied and is best when the exterior fluid is more viscous. For $\Lambda < 1$, the fit is improved by using an interpolation based upon an arithmetic mean of viscosities however the fit at $\Lambda > 1$ then degrades. Over the range of Λ, the scheme in Eq. (27) produced most consistent agreement.

Comparison with the Taylor-Einstein represents a stringent test of phase field MCLBE (and thereby the approximations within the theory [10], which, here, has been extended to fluid subject to an immersed boundary force [9]). It is facilitated by our development of an inverse MRT methodology—a generic scheme which circumvents the need for a calculation of collision matrix and allows direct construction of a post-collision LBE distribution function.

The conditions of our validation (Re, Ca small) mean the microcurrent is significant with respect of physical flow (possibly the reason for previous neglect of this validation). Our results achieve a paradoxical accuracy resolved by appealing to recent work on the hydrodynamic nature of microcurrent flow [27], the accuracy of the Taylor-Einstein result recovered herein may be understood by observing that $\text{Re} = 0$ regime is linear and microcurrent stresses (themselves a solution of the Stokes equation) therefore superpose with flow induced by the applied shear. Once identified, they may be subtracted. Furthermore, this work points to the importance of the method of interpolation of viscosity eigenvalue, λ_4, across the interfacial region, with our data producing a optimum for the interpolation in Eq. (27).

ACKNOWLEDGMENTS

M.A.E. gratefully acknowledges financial support from the Engineering and Physical Sciences Research Council, Swindon, UK via a summer bursary from Collaborative Computational Project 5, Grant Reference EP/M022617/1 and Oriel College, University of Oxford.

[1] P. Lallemand and L.-S. Luo, Phys. Rev. E **61**, 6546 (2000).
[2] R. Benzi, S. Succi, and M. Vergassola, Europhys. Lett. **13**, 727 (1990).
[3] R. Benzi, S. Succi, and M. Vergassola, Phys. Rep. **222**, 145 (1992).
[4] P. J. Dellar, Phys. Rev. E **65**, 036309 (2002).
[5] M. E. McCracken and J. Abraham, Phys. Rev. E **71**, 036701 (2005).
[6] K. N. Premnath and J. Abraham, J. Comput. Phys. **224**, 539 (2007).
[7] R. Du, B. Shi, and X. Chen, Phys. Lett. A **359**, 564 (2006).
[8] A. Fakhari and T. Lee, Phys. Rev. E **87**, 023304 (2013).
[9] I. Halliday, X. Xu, and K. Burgin, Phys. Rev. E **95**, 023301 (2017).
[10] G. I. Taylor, Proc. Roy. Soc. **138**, 41 (1932).
[11] E. Einstein, Ann. Physik. **19**, 371 (1906).
[12] Y. H. Qian, D. d'Humières, and P. Lallemand, Europhys. Lett. **17**, 479 (1992).
[13] H. Liu, A. J. Valocchi, and Q. Kang, Phys. Rev. E **85**, 046309 (2012).
[14] Y. Ba, H. Liu, J. Sun, and R. Zheng, Phys. Rev. E **88**, 043306 (2013).
[15] S. V. Lishchuk, C. M. Care, and I. Halliday, Phys. Rev. E **67**, 036701 (2003).
[16] U. D'Ortona, D. Salin, M. Cieplak, R. B. Rybka, and J. R. Banavar, Phys. Rev. E **51**, 3718 (1995).
[17] L. Landau and E. M. Lifshitz, *Fluid Mechanics*, 2nd ed. (Pergamon Press, Oxford, UK, 1966)
[18] H. Liu, A. J. Valocchi, C. Werth, Q. Kang, and M. Oostrom, Adv. Water Resour. **73**, 144 (2014).
[19] H. Liu, Y. Ju, N. Wang, G. Xi, and Y. Zhang, Phys. Rev. E **92**, 033306 (2015).
[20] I. Ginzburg, J. Stat. Phys. **126**, 157 (2007).
[21] Y. Q. Zu and S. He, Phys. Rev. E **87**, 043301 (2013).
[22] D. Grunau, S. Chen, and K. Eggert, Phys. Fluids A **5**, 2557 (1993).
[23] T. J. Spencer, I. Halliday, and C. M. Care, Phys. Rev. E **82**, 066701 (2010).
[24] M. A. Nawab and S. G. Mason, Trans. Faraday Soc. **54**, 1712 (1958).
[25] B. K. Hur, C. B. Kim, and C. G. Lee, J. Ind. Eng. Chem. **6**, 318 (2000).
[26] T. G. Mason, J. Bibette, and D. A. Weitz, J. Colloid Interface Sci. **179**, 439 (1996).
[27] I. Halliday, S. V. Lishchuk, T. J. Spencer, K. Burgin, and T. Schenkel, Comput. Phys. Commun. **219**, 286 (2017).
[28] A. J. Wagner and I. Pagonabarraga, J. Stat. Phys. **107**, 521 (2002).